Journal of Power Sources 196 (2011) 10758–10761

Contents lists available at SciVerse ScienceDirect

Journal of Power Sources

journal homepage: www.elsevier.com/locate/jpowsour

Short communication

Mesoporous nano-Co_3O_4: A potential negative electrode material for alkaline secondary battery

Li Li[a], Yaping Wang[b], Yijing Wang[a,*], Yan Han[a], Fangyuan Qiu[a], Guang Liu[a], Chao Yan[a], Dawei Song[c], Lifang Jiao[a], Huatang Yuan[a]

[a] Institute of New Energy Material Chemistry, Key Laboratory of Advanced Energy Materials Chemistry (MOE), Nankai University, Tianjin 300071, PR China
[b] Center of Photonics Fabrication, Jiangsu University, Zhenjiang 212013, PR China
[c] School of Chemistry and Chemical Engineering, Henan University of Technology, Zhengzhou 450001, PR China

ARTICLE INFO

Article history:
Received 27 January 2011
Received in revised form 30 June 2011
Accepted 22 August 2011
Available online 27 August 2011

Keywords:
Mesoporous
Nano-Co_3O_4
Active starting material
Electrochemical performance
Alkaline secondary battery

ABSTRACT

A potential negative electrode material (mesoporous nano-Co_3O_4) is synthesized via a simple thermal decomposition of precursor $Co(OH)_2$ hexagonal nanosheets in the air. The structure and morphology of the samples are characterized by X-ray diffraction (XRD), scanning electron microscopy (SEM) and transmission electron microscopy (TEM). It is found that the nano-Co_3O_4 is present in mesoporous hexagonal nanoparticles. The average size of holes is about 5–15 nm. The electrochemical performances of mesoporous nano-Co_3O_4 as the active starting negative electrode material for alkaline secondary battery are investigated by galvanostatic charge–discharge and cyclic voltammetry (CV) technique. The results demonstrate that the prepared mesoporous nano-Co_3O_4 electrode displays excellent electrochemical performance. The discharge capacity of the mesoporous nano-Co_3O_4 electrode can reach 436.5 mAh g^{-1} and retain about 351.5 mAh g^{-1} after 100 cycles at discharge current of 100 mA g^{-1}. A properly electrochemical reaction mechanism of mesoporous nano-Co_3O_4 electrode is also constructed in detail.

1. Introduction

To meet the ever-increasing demands for spacecrafts, communication, computers, electric vehicles, cellular phones, camcorders, power tools and other home appliances, there are continuous demands to develop rechargeable batteries with high power densities. Nickel-based rechargeable batteries, such as nickel–cadmium (Ni/Cd), nickel–metal hydride (Ni/MH), nickel–iron (Ni/Fe) and nickel–zinc (Ni/Zn) batteries [1–9], are widely used in many areas for their high energy and power densities. Recently, a new type of nickel-based rechargeable battery named nickel–cobalt (Ni/Co) battery has drawn much attention for its high discharge capacities, good cycling stability and excellent high-rate performances. In this battery system, the reversible capacity is mainly based on the faradaic redox mechanism between $Co(OH)_2$ and metallic Co. The charge–discharge reaction can be expressed as follows [10,11]:

$$Co + 2OH^- \underset{\text{Charge}}{\overset{\text{Discharge}}{\rightleftharpoons}} Co(OH)_2 + 2e$$

Thus, Co, $Co(OH)_2$ or those cobalt-based compounds which can be transformed into Co or $Co(OH)_2$ in alkaline electrolyte are all potential negative materials. Up to now, some cobalt-based compounds, such as $Co(OH)_2$ [11,12], Co–B [13], Co–P [14], Co–Si [15], Co–S [16], and CoO [17] have been proved to be suitable for Ni/Co battery. Other cobalt-based compounds, such as Co_3O_4, are possible negative materials although they have not yet been sufficiently investigated.

Mesoporous materials have evoked increased interest because of their potential applications in chemical separation, energy storage and conversion, catalysis, microelectronics and optics. Mesoporous materials are widely used in battery system, especially in lithium ion battery [18–21]. However, few studies have been reported on the electrochemical properties of mesoporous materials for Ni/Co battery. In our previous work, it is found that increasing the contact area with alkaline electrolyte is very important to improve the electrochemical performances of $Co(OH)_2$ for Ni/Co battery [22]. The porosity of mesoporous materials can provide the channels for electrolyte which are obviously useful to increasing the contact area between active materials and electrolyte. Thus, they must be effective negative materials for alkaline secondary battery.

In this paper, we firstly report the use of mesoporous nano-Co_3O_4 negative materials in alkaline secondary battery. The structural and electrochemical characteristics of mesoporous nano-Co_3O_4 are investigated in detail. Moreover, the electrochemical reaction mechanism is discussed.

* Corresponding author. Tel.: +86 22 23503639; fax: +86 22 23503639.
E-mail address: wangyj@nankai.edu.cn (Y. Wang).

0378-7753/$ – see front matter © 2011 Elsevier B.V. All rights reserved.
doi:10.1016/j.jpowsour.2011.08.086

2. Experimental

2.1. Preparation of mesoporous nano-Co_3O_4 particles

Mesoporous nano-Co_3O_4 was synthesized by a simple thermal decomposition of $Co(OH)_2$ in air. In the typical synthesis, $CoCl_2{\cdot}6H_2O$ (10 mmol, 98.0–102.0%, Alfa Aesar) was dissolved into 50 ml distilled water to form a homogeneous solution under magnetic stirring within 30 min. An appropriate amount of sodium hydroxide dissolved in 20 ml distilled water was dropwise into the above solution under magnetic stirring within 5 min. The brown precipitation was centrifuged, washed with distilled water and absolute alcohol, and dried at 60 °C in vacuum for 12 h. Finally, the precipitation was heated at 400 °C for 1 h in the air and slowly cooled to room temperature.

2.2. Structural and morphological characterization

The crystal structure and surface morphology of the as-prepared $Co(OH)_2$ and mesoporous nano-Co_3O_4 were characterized by X-ray diffraction (XRD, Rigaku D/Max-2500, Cu Kα radiation), scanning electron microscopy (SEM, S-3500N), transmission electron microscopy (TEM, Tecnai 20). The BET surface area was measured by Tristar 3000.

2.3. Electrochemical measurements

Negative electrodes were constructed through mixing as-prepared mesoporous nano-Co_3O_4 with carbonyl nickel powders in a weight ratio of 1:3. The powder mixture was pressed under 30 MPa of pressure into a small pellet of 10 mm diameter and 1.5 mm thickness. The pellet was then pressed under 20 MPa of pressure between two pieces of Ni foam. Electrochemical measurements were conducted in a three compartment cell using a Land battery test instrument (CT 2001A). $NiOOH/Ni(OH)_2$ and Hg/HgO were used as the counter electrode and the reference electrode, respectively. The electrolyte was a 6 M KOH aqueous solution. The electrodes were charged at 200 mA g^{-1} for 3 h, discharged at 100 mA g^{-1} to −0.5 V (vs. Hg/HgO). The testing interval between charge and discharge was 5 min.

The cyclic voltammetry (CV) was conducted by using electrochemical workstation (Zahner IM6e). The potential scan rate was 0.2 mV s^{-1} and the scan scope was −1.2 V to −0.4 V.

3. Results and discussion

3.1. Characterization of structure and morphology

Fig. 1 exhibits the XRD patterns of the precursor β-$Co(OH)_2$ (a) and mesoporous nano-Co_3O_4 (b). All the diffraction peaks of samples a and b in Fig. 1 can be indexed to the hexagonal phase of brucitelike β-$Co(OH)_2$ (space group $P\bar{3}ml$, JCPDS, No. 74-1057) and the cubic phase of Co_3O_4 (space group Fd-3m, JCPDS, No. 73-1701), respectively. The sharp diffraction peaks (Fig. 1b) suggest crystalline nature of the mesoporous nano-Co_3O_4. The lattice parameters $a = b = c = 8.076$ Å from the diffraction pattern are in good agreement with the standard values for cubic Co_3O_4. No other diffraction peaks can be observed, indicating a pure phase of Co_3O_4.

Fig. 2 shows the SEM images of the precursor β-$Co(OH)_2$ (a) and mesoporous nano-Co_3O_4 (b), respectively. The SEM image in Fig. 2a illustrates that the as-prepared precursor $Co(OH)_2$ is mainly composed of hexagonal nanosheets. In addition, the SEM image of the mesoporous nano-Co_3O_4 (Fig. 2b) clearly shows that the size and shape of the mesoporous nano-Co_3O_4 nanosheets are consistent with the $Co(OH)_2$, but the surface of the nanosheets is not very smooth. Further insight into the morphology and microstructure of

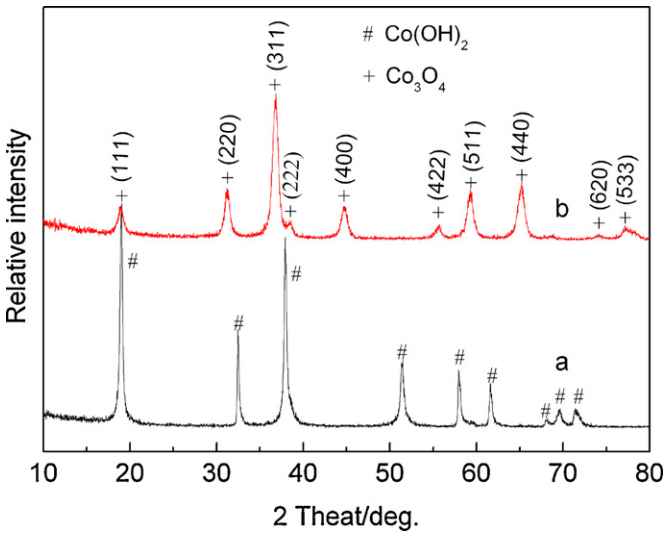

Fig. 1. XRD patterns of β-$Co(OH)_2$ (a) and mesoporous nano-Co_3O_4 (b).

the mesoporous nano-Co_3O_4 is gained by using transmission electron microscopy (TEM). As shown in Fig. 3, the porous nanosheets can be clearly observed, and the nano-Co_3O_4 is present in mesoporous hexagonal nanoparticles with the average size around 100 nm. Besides, the average size of holes is about 5–15 nm, and the shape of holes is irregular. The formation of mesopores may be attributed to the impact of gas evolution during the thermal

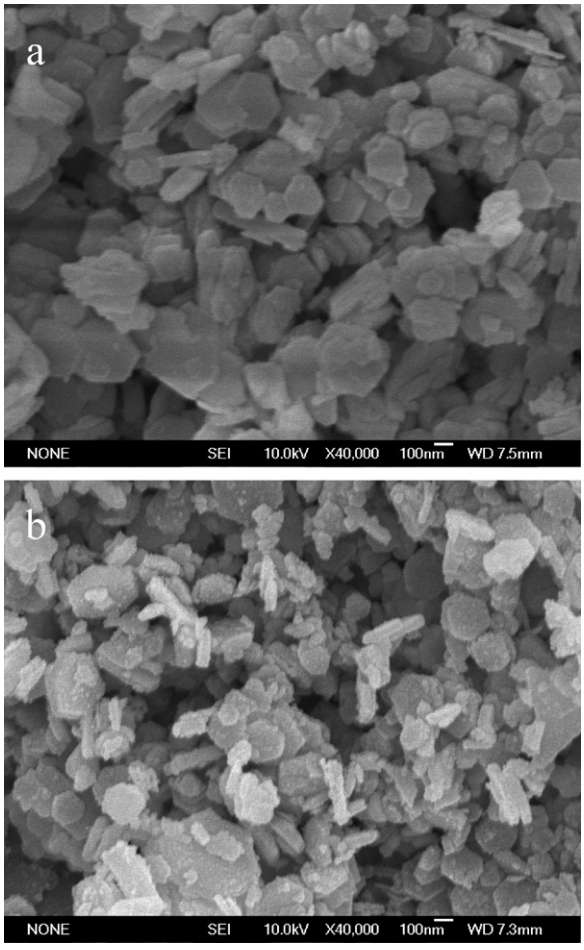

Fig. 2. SEM images of β-$Co(OH)_2$ (a) and mesoporous nano-Co_3O_4 (b).

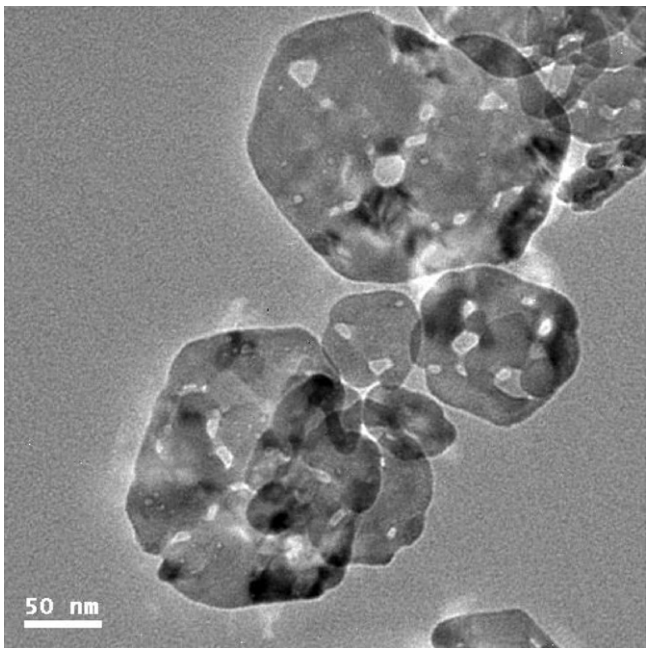

Fig. 3. TEM image of mesoporous nano-Co_3O_4.

decomposition reaction of the precursor β-$Co(OH)_2$ nanosheets. This kind of mesoporous structure possesses relatively large mesotunnels inside the pore walls, which may be facilitate to improve its electrochemical performances.

Specific surface area is measured by BET method. The specific surface areas of β-$Co(OH)_2$ and nano-Co_3O_4 are 48.73 $m^2\,g^{-1}$ and 64.85 $m^2\,g^{-1}$, respectively. The higher specific surface areas of nano-Co_3O_4 should be attributed to the pores in the hexagonal sheets.

3.2. Electrochemical performance

Fig. 4 shows the cycle life of the mesoporous nano-Co_3O_4 and precursor β-$Co(OH)_2$ electrodes at a constant discharging current of 100 mA g^{-1}. As it can be seen, the maximum discharge capacity of β-$Co(OH)_2$ electrode reaches 471.9 mAh g^{-1} at the first cycle and decreases gradually in the following charge–discharge cycles. After 100 charge–discharge cycles, the reversible discharge capacity maintains about 258.5 mAh g^{-1}. For the nano-Co_3O_4 electrode,

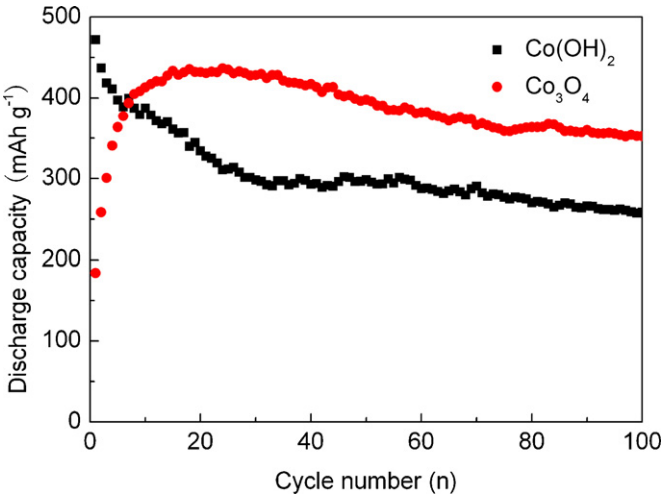

Fig. 4. Cycle life of mesoporous nano-Co_3O_4 and β-$Co(OH)_2$ electrodes.

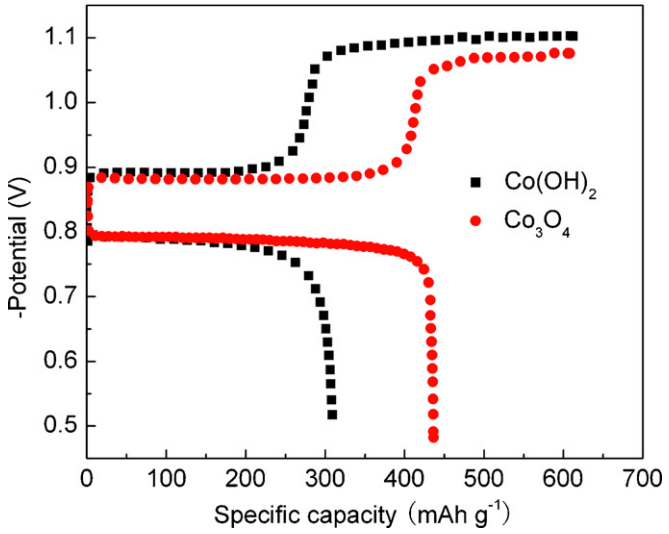

Fig. 5. Charge–discharge curves of mesoporous nano-Co_3O_4 and β-$Co(OH)_2$ electrodes at the 24th cycle.

it is noted that the electrode has an activation process. The discharge capacity gradually increases at the initial few cycles. At the 24th cycle, the maximum discharge capacity of 436.5 mAh g^{-1} is observed. Then, the discharge capacity decreases gradually in the initial 75 charge–discharge cycles and keeps stable after 75 cycles. The reversible discharge capacity maintains about 351.5 mAh g^{-1} after 100 charge–discharge cycles, which is much higher than that of β-$Co(OH)_2$ electrode. Obviously, nano-Co_3O_4 electrode shows better cycle performance as compared to the precursor β-$Co(OH)_2$ electrode.

Fig. 5 shows the 24th cycle charge–discharge curves of the mesoporous nano-Co_3O_4 and precursor β-$Co(OH)_2$ electrodes at the charge current of 200 mA g^{-1} and discharge current of 100 mA g^{-1}, respectively. As shown in Fig. 5, the potential plateaus positions and curves shapes of the two electrodes are nearly the same. For each electrode, there are only one charge plateau and one discharge plateau, which can be observed at about −0.88 V and −0.78 V, respectively. In addition, it is also noted that the length of charge plateaus and discharge plateaus in mesoporous nano-Co_3O_4 electrode is almost the same, suggesting the excellent reversibility.

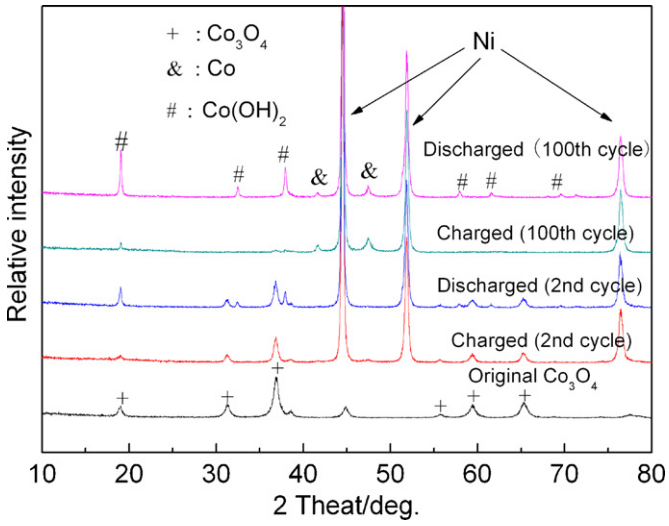

Fig. 6. XRD patterns of mesoporous nano-Co_3O_4 electrode at different cycles.

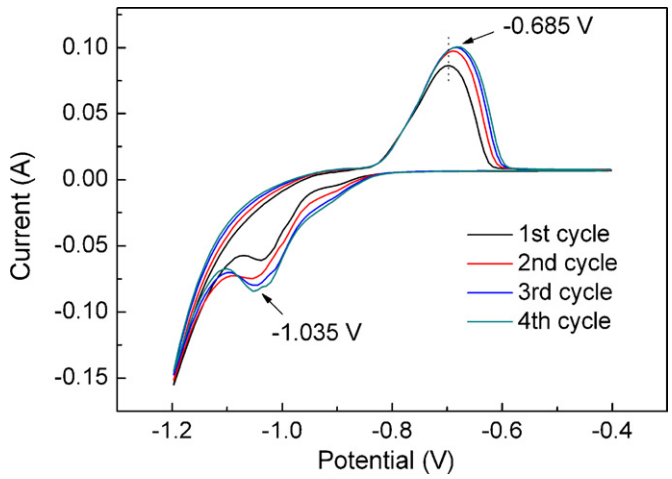

Fig. 7. CV curves of mesoporous nano-Co_3O_4 electrode in the initial 4 cycles at a scan rate of 2 mV s^{-1}.

To investigate the structure change in charge–discharge process, XRD patterns of mesoporous nano-Co_3O_4 electrode at different cycles are compared in Fig. 6. At the fully charged state of the 2nd cycle, the diffraction peaks of the Co_3O_4 become weak and the peaks of Co appear, indicating the formation of Co during the charging process. When discharged to −0.5 V, it can be found that the diffraction peaks of β-$Co(OH)_2$ are detected. Besides, the diffraction peaks of metallic Co are detected at the fully charged state in the 100th cycle. At the fully discharged state in the 100 cycle, most of the diffraction peaks can be indexed as $Co(OH)_2$ and the diffraction peaks of the metallic Co become weak. It can be concluded that β-$Co(OH)_2$ is reduced to metallic Co during the charge process, and metallic Co is oxidated to β-$Co(OH)_2$ during the discharge process. According to the intensity change of diffraction peaks of Co_3O_4, Co and β-$Co(OH)_2$ at different cycles, there may be a transformation from Co_3O_4 to β-$Co(OH)_2$ during the initial 24 cycles. When Co_3O_4 transforms completely into Co or β-$Co(OH)_2$, the discharge capacity of electrode reaches the maximum of 436.5 mAh g^{-1}. The discharge capacity of the electrode after activation process is mainly attributed to the electrochemical redox reaction between Co and $Co(OH)_2$. That is to say, the negative electrode material is really nano sized Co metal particles derived from the electrochemical reduction of nano-Co_3O_4. We can see from Fig. 4 that the reversible discharge capacity of nano-Co_3O_4 is about 351.5 mAh g^{-1} in the 100th cycle. If this is re-calculated based on the starting weight of β-$Co(OH)_2$, the discharge capacity (303.6 mAh g^{-1}) is higher than that of precursor β-$Co(OH)_2$ (258.5 mAh g^{-1}). Thus, the discharge capacity of nano-Co_3O_4 is enhanced. The capacity utilization may be related to the mesoporous nano-active starting negative material.

Fig. 7 shows the cyclic voltammogram (CV) curves of the mesoporous nano-Co_3O_4 electrode at the initial four cycles in 6 M KOH aqueous solution. It can be seen that there is an activation process in the CV curves. The integral area of the redox peaks increases gradually and peak voltage of the redox peaks shifts gradually right. The pair of remarkable reduction–oxidation peaks appears at −1.035 V and −0.685 V in the fourth CV cycle, respectively, suggesting a reversible electrochemical oxidation–reduction process occurring on the mesoporous nano-Co_3O_4 electrode.

4. Conclusions

In summary, mesoporous nano-Co_3O_4 with a hexagonal sheetlike structure has been prepared by a simple thermal decomposition of precursor $Co(OH)_2$ hexagonal nanosheets. The electrochemical performances of mesoporous nano-Co_3O_4 are firstly investigated as active starting negative electrode material for alkaline secondary battery. The results exhibit that the discharge capacity can reach 436.5 mAh g^{-1} and still remain at 351.5 mAh g^{-1} after 100 cycles. Most of the discharge capacity can be attributed to the redox reaction between Co and $Co(OH)_2$. If nano-Co_3O_4 transforms completely to β-$Co(OH)_2$ by calculation, the reversible discharge capacity (303.6 mAh g^{-1}) is higher than that of precursor β-$Co(OH)_2$ (258.5 mAh g^{-1}). Thus, the as-synthesized mesoporous nano-Co_3O_4 is a promising active starting negative electrode material for alkaline secondary battery.

Acknowledgements

This work was financially supported by MOST project (2010CB631303), NSFC (50971071, 51071087), MOE (IRT-0927), Nature Science Foundation of Tianjin (11JCYBJC07700, 09JCZDJC24800) and Tianjin Sci & Tech (10SYSYJC27600).

References

[1] X.Y. Xiong, H. Vander Poorten, M. Crappe, Electrochim. Acta 41 (1996) 1267–1275.
[2] S.R. Ovshinsky, M.A. Fetcenko, J. Ross, Science 260 (1993) 176–181.
[3] W. Yin, M. Zhao, Electrochim. Acta 52 (2007) 2723–2728.
[4] K. Vijayamohanan, T.S. Balasubramanian, A.K. Shukla, J. Power Sources 34 (1991) 269–285.
[5] Y.F. Liu, H.G. Pan, M.X. Gao, Y.F. Zhu, Y.Q. Lei, Q.D. Wang, Electrochim. Acta 49 (2004) 545–555.
[6] J. Jindra, J. Power Sources 66 (1997) 15–25.
[7] Y.F. Yuan, J.P. Tu, H.M. Wu, Y.Z. Yang, D.Q. Shi, X.B. Zhao, Electrochim. Acta 51 (2006) 3632–3636.
[8] X. Zhao, L. Ma, Y. Yao, Y. Ding, X. Shen, Energy Environ. Sci. 3 (2010) 1316–1321.
[9] X.P. Gao, H.X. Yang, Energy Environ. Sci. 3 (2010) 174–189.
[10] P. Elumalai, H.N. Vasan, N. Munichandraiah, J. Power Sources 93 (2001) 201–208.
[11] X.P. Gao, S.M. Yao, T.Y. Yan, Z. Zhou, Energy Environ. Sci. 2 (2009) 502–505.
[12] S.M. Han, Z.H. Feng, L. Hu, Y. Li, J.S. Hao, J.W. Zhang, Mater. Chem. Phys. 124 (2010) 17–20.
[13] Y.D. Wang, X.P. Ai, H.X. Yang, Chem. Mater. 16 (2004) 5194–5197.
[14] Y.L. Cao, W.C. Zhou, X.Y. Li, X.P. Ai, X.P. Gao, H.X. Yang, Electrochim. Acta 51 (2006) 4285–4290.
[15] Y.H. Zhang, L.F. Jiao, Y.J. Wang, Q.H. Wang, Y.Y. Zhang, L. Liu, H.T. Yuan, Int. J. Hydrogen Energy 33 (2008) 4819–4823.
[16] D.W. Song, Q.H. Wang, Y.P. Wang, Y.J. Wang, Y. Han, L. Li, G. Liu, L.F. Jiao, H.T. Yuan, J. Power Sources 195 (2010) 7462–7465.
[17] Y. Yu, G.B. Ji, J.M. Cao, J.S. Liu, M.B. Zheng, J. Alloys Compd. 471 (2009) 268–271.
[18] Y.F. Shi, B.K. Guo, S.A. Corr, Q.H. Shi, Y.-S. Hu, K.R. Heier, L.Q. Chen, R. Seshadri, G.D. Stucky, Nano Lett. 9 (2009) 4215–4220.
[19] F.M. Zhan, B.Y. Geng, Y.J. Guo, Chem. Eur. J. 15 (2009) 6169–6174.
[20] H. Liu, G.X. Wang, J. Liu, S.Z. Qiao, H. Ahn, J. Mater. Chem. 21 (2011) 3046–3052.
[21] D.Q. Shi, J.P. Tu, Y.F. Yuan, H.M. Wu, Y. Li, X.B. Zhao, Electrochem. Commun. 8 (2006) 1610–1614.
[22] D.W. Song, Y.J. Wang, Q.H. Wang, Y.P. Wang, L.F. Jiao, H.T. Yuan, J. Power Sources 195 (2010) 7115–7119.